The small molecule tool (*S*)-(−)-blebbistatin: novel insights of relevance to myosin inhibitor design†

Cristina Lucas-Lopez,‡[a] John S. Allingham,‡§[b] Tomas Lebl,[a] Christopher P. A. T. Lawson,[a] Ruth Brenk,[c] James R. Sellers,[d] Ivan Rayment*[b] and Nicholas J. Westwood*[a]

Received 23rd January 2008, Accepted 25th March 2008
First published as an Advance Article on the web 21st April 2008
DOI: 10.1039/b801223g

The small molecule blebbistatin is now a front line tool in the study of myosin function. Chemical modification of the tricyclic core of blebbistatin could deliver the next generation of myosin inhibitors and to help address this we report here on the impact of structural changes in the methyl-substituted aromatic ring of blebbistatin on its biological activity. Chemical methods for the preparation of isomeric methyl-containing analogues are reported and a series of co-crystal structures are used to rationalise the observed variations in their biological activity. These studies further support the view that the previously identified binding mode of blebbistatin to *Dictyostelium discoideum* myosin II is of relevance to its mode of action. A discussion of the role that these observations have on planning the synthesis of focused libraries of blebbistatin analogues is also provided including an assessment of possibilities by computational methods. These studies are ultimately directed at the development of novel myosin inhibitors with improved affinity and different selectivity profiles from blebbistatin itself.

Introduction

The investigation of normal and aberrant cellular function is greatly enhanced by chemical tools that precisely and rapidly inhibit specific targets in a defined manner. These tools are particularly valuable for dissecting complex cellular processes such as cytokinesis.[1] Thus the recent discovery that (*S*)-(−)-blebbistatin (**1**) (Scheme 1) inhibits a limited number of myosin II isoforms has allowed the role of these myosins to be assessed in a wide range of cellular processes including cytokinesis[1] and cellular migration[2] in a manner that was previously inaccessible. As such **1** represents an exciting addition to the strategies available for studying the cytoskeleton *in vivo*. Importantly, the introduction of **1** has allowed the focus to shift from small molecule ligand interactions with actin[3] to the control of individual classes of motor proteins.

At present more than 18 classes of myosin have been recognised by phylogenetic analyses[4] and all are characterised by the presence of a motor domain that interacts with actin, hydrolyzes ATP, and mediates a nucleotide-dependent conformational change that results in directed movement. For the most part they share the same chemical mechanism and given this commonality would not be expected to be good targets for individual chemical regulation. However, a series of functional, kinetic and structural investigations have shown that (*S*)-(−)-blebbistatin (**1**) achieves

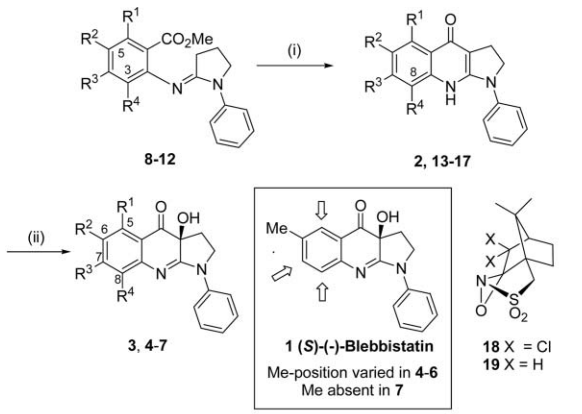

Substituent R^1-R^4				Compound #			e.e./reagent[b]	
R^1	R^2	R^3	R^4		**2**[a]	**3**[a]	**18**	**19**
Me	H	H	H	**8**	**13**	**4**	64	17
H	Me	H	H	**9**	**14**	**1**	86[c]	42[c]
H	H	Me	H	**10**	**15**	**5**	90	28
H	H	H	Me	**11**	**16**	**6**	86	40
H	H	H	H	**12**	**17**	**7**	86	55

Scheme 1 Numbering scheme and chemical structures of analogues **4**–**7** and their synthetic precursors. *Reagents and conditions*: for the synthesis of **8**–**12**, including yields, see Experimental section; (i) LiHMDS, THF, **13** (84%), **14** (90%)[9], **15** (95%), **16** (95%), **17** (95%); (ii) LiHMDS, THF, oxaziridine **18** or **19**; for **18**, **4** (87% yield), **1** (82%)[9], **5** (83%), **6** (63%), **7** (78%); for yields using **19** see Experimental section. [a]Generalised structures used to represent a particular stage in the synthesis process. [b]Observed enantiomeric excess (ee) as a function of substrate and structure of the oxaziridine used. [c]See ref. 9 for details.

[a]*School of Chemistry and the Centre for Biomolecular Sciences, University of St Andrews, North Haugh, St Andrews, Fife, UK KY16 9ST. E-mail: njw3@st-andrews.ac.uk*
[b]*Department of Biochemistry, University of Wisconsin, Madison, WI 53706, USA. E-mail: ivan_rayment@biochem.wisc.edu*
[c]*Division of Biological Chemistry and Drug Discovery, College of Life Sciences, University of Dundee, Dow Street, Dundee, UK DD1 5EH*
[d]*Laboratory of Molecular Physiology, National Heart, Lung and Blood Institute, National Institutes of Health, Bethesda, MD 20892-1762, USA*
† Electronic supplementary information (ESI) available: More detailed discussion regarding cyclisation of **11**; biological activity of (*S*)-(−)-blebbistatin analogues; data collection and refinement statistics for the co-crystal structures of S1dC with **4**–**7**. See DOI: 10.1039/b801223g
‡ These authors contributed equally to this work.
§ Current Address: Department of Biochemistry, Queen's University, Kingston, ON, K7L 3N6, Canada.

selectivity by binding in a highly hydrophobic cleft in the myosin motor domain.[5–8] Surprisingly, this is one of the most conserved components of all myosin motor domains where a few small sequence and structural differences lead to the ability of **1** to discriminate between myosin isoforms.

Given our detailed knowledge of the molecular interactions of (*S*)-(−)-blebbistatin (**1**) with non-muscle myosin II, there is every reason to believe that additional biological tools can be synthesised with improved potency and specificity. In particular it is ultimately desirable to design, or select from libraries of analogues, ligands that can discriminate between distinct classes of myosin. Our initial approach has been to carry out chemical optimisation studies on **1** coupled closely with biochemical, computational and X-ray crystallographic analysis of the impact of any structural changes. We have previously reported that a nitro-functional group can be incorporated into the core structure of **1** without significant loss of activity and that this leads to a dramatic improvement in the light stability of **1**.[9]

Results and discussion

Analysis of the co-crystal structure of 1 bound to S1dC

The recently reported co-crystal structure of (*S*)-(−)-blebbistatin (**1**) bound to the metastable state of *Dictyostelium discoideum* myosin II (S1dC) provided an explanation for its mechanism of inhibition and specificity at a molecular level.[8] It showed that **1** binds near the apex of the 50 kDa cleft of myosin (Fig. 1a). The structure also revealed that, in part, binding of **1** is stabilised, and perhaps its orientation controlled, by the formation of a hydrogen bonding network between the main chain carboxylate oxygen of Leu262, the main chain amide hydrogen of Gly240, and the hydroxyl group of the (*S*)-(−)-enantiomer (Fig. 1b).[8] However, most of the binding strength seems to be controlled by the 'hydrophobic effect' as the blebbistatin binding pocket encloses the largely hydrophobic compound in a complimentary hydrophobic environment. For example, the *N*-phenyl ring–myosin II interface is comprised of residues Leu262, Phe466, Glu467, Cys470, and Val630, whilst the tricyclic core interacts with Tyr261, Ser456, Ile471, Thr474, Tyr634, Gln637, Leu638, and Leu641 (Fig. 1b).

The methyl-containing aromatic ring of (*S*)-(−)-blebbistatin (**1**) interacts with the deepest point of the 50 kDa cleft (Fig. 1 and 2). Based on the position of this ring and the surrounding hydrophobic residues, the location of the attached methyl group is predicted to have a significant influence on the molecular complementarity of the ligand–protein interface, and thus the affinity for its binding site in S1dC myosin II. In order to probe the effects of structural changes in this portion of **1** on myosin inhibition, a series of analogues of **1** have been synthesised that differ in the position (or existence) of the methyl group.

(*S*)-(−)-Blebbistatin (1) analogue synthesis

We have recently established a synthetic route to analogues of **1** using Davis' asymmetric hydroxylation methodology to convert quinolones of the general type **2** to the corresponding α-hydroxy ketones **3** (Scheme 1).[9] Whilst the route was sufficiently robust to enable the synthesis of analogues **4–7** of **1**, several interesting differences were observed across the series. First, the ease of

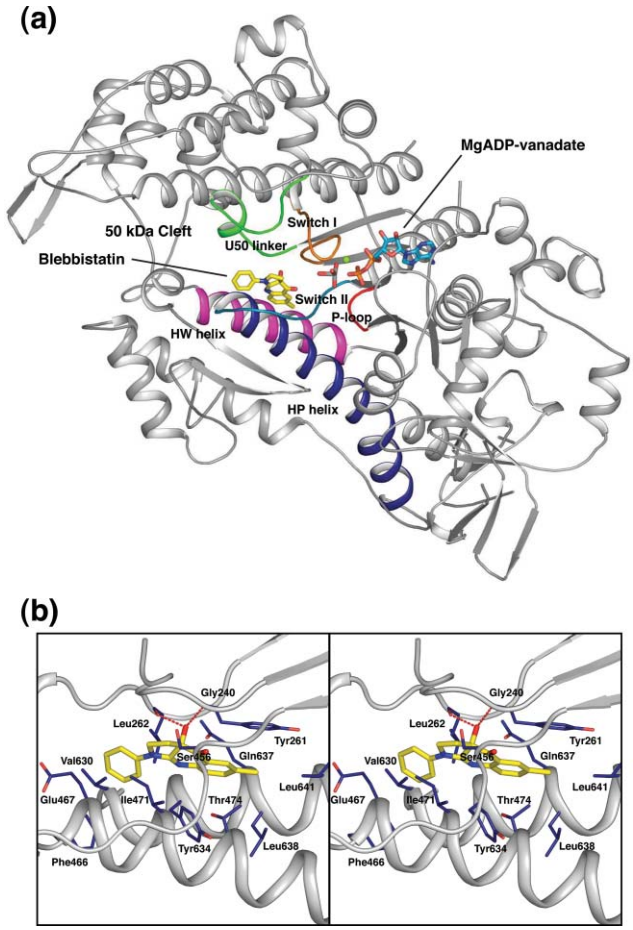

Fig. 1 Structure of the *Dictyostelium discoideum* myosin II S1dC–MgADP–vanadate–(*S*)-(−)-blebbistatin (**1**) complex. (a) Myosin is shown as a ribbon diagram (grey) with nucleotide (blue carbon and nitrogen atoms) and (*S*)-(−)-blebbistatin (**1**) (yellow carbon atoms) bound at their respective sites (PDB accession: 1YV3). The binding pocket of **1** is formed by the U50 linker (green) from the upper face of the 50 kDa cleft and the HP (blue) and HW (pink) helices, which form part of the lower face of the 50 kDa cleft.[10] (b) Stereoview of the blebbistatin binding site showing the hydrogen bonding interactions and largely hydrophobic nature of the interface residues (side chains of these residues are shown with blue carbon atoms and red oxygen atoms).

formation of the amidines **8–12** varied with the position of the methyl-substituent with the synthesis of the 5-substituted amidine **9** (R^2 = Me, Scheme 1) being the most efficient, presumably reflecting the increased nucleophilicity of the aniline nitrogen in the starting anthranilate. In contrast, the sterically encumbered 3-methyl-substituted amidine **11** (R^4 = Me) was formed in low yield under reaction conditions analogous to those used in the synthesis of **9**. Sufficient quantities of **11** could be prepared following a significant increase in the reaction time. Second, the cyclisation conditions required to convert the amidines **8–12** to the corresponding quinolones **13–17** (Scheme 1) varied as a function of structure with yields of 84–95% being obtained in 3 h at 0 °C for quinolones **13–15** and **17**. However, it was necessary to increase the temperature and the reaction time to prepare quinolone **16** in 95% yield probably reflecting a strong preference for a conformation of the lithium anion of **11** that minimizes the interaction between the 3-methyl and N–Li groups (Scheme 1).†

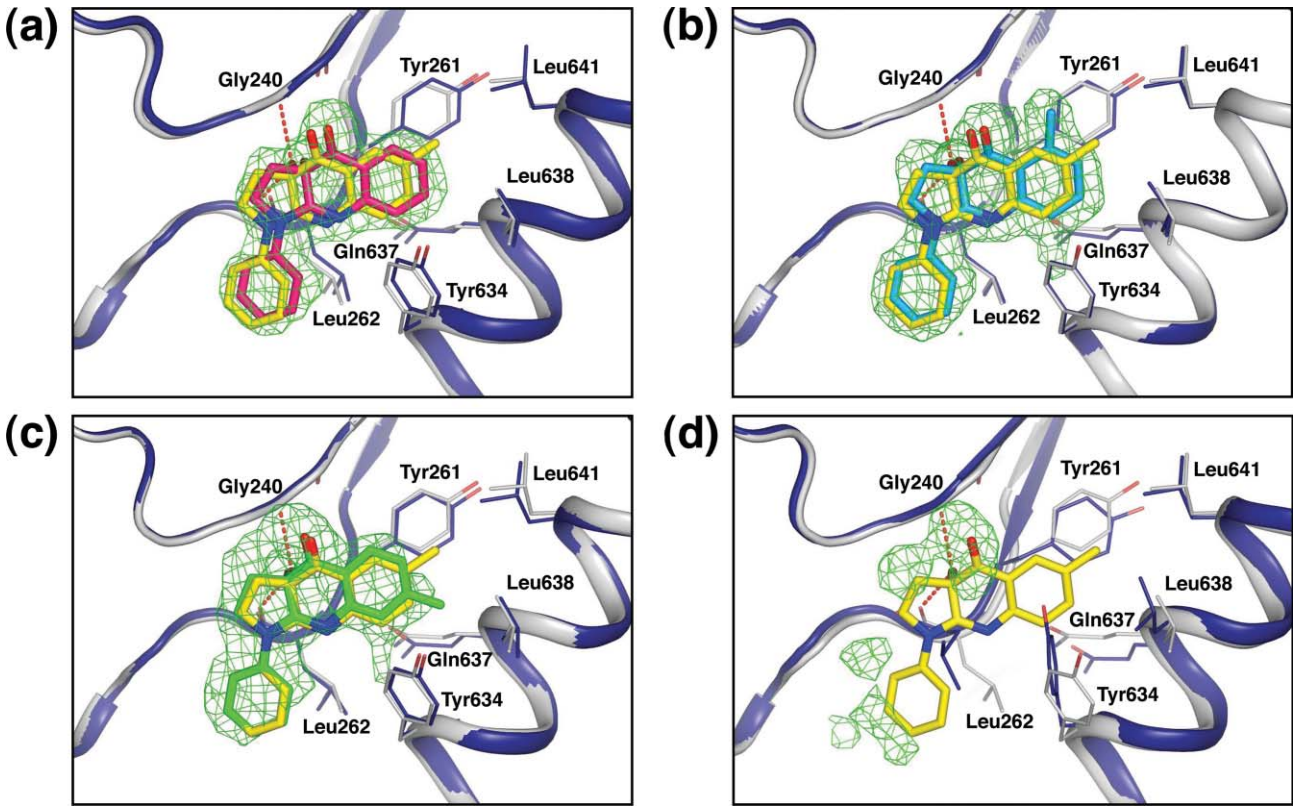

Fig. 2 Overlays of the *Dictyostelium discoideum* myosin II S1dC–MgADP–vanadate binding pocket structures for (*S*)-(−)-blebbistatin (**1**) and each of the blebbistatin analogues (PDB accession: 3BZ7, 3BZ8, 3BZ9). The X-ray crystal structures of the myosin's interaction with (a) analogue **7** (pink carbon atoms), (b) analogue **4** (light blue carbon atoms), (c) analogue **5** (green carbon atoms), and (d) the electron density observed on incubation with analogue **6** are shown superimposed upon the original ternary structure of **1** (yellow carbon atoms in all cases). All alignments were performed by superimposing the α-carbon atoms for the analogue-bound form of myosin (blue) onto the (*S*)-(−)-blebbistatin (**1**)-bound form (white). Selected residues that form the inhibitor–myosin interface are shown. Electron density maps contoured at 3σ are shown for all analogue complexes (green mesh). The maps were calculated with coefficients of the form $F_o - F_c$ where the inhibitor was omitted from the refinement and phase calculation. For two of the complexes [myosin-**4** and -**5**, (b) and (c) respectively], an additional area of electron density was observed in the region of the 8-position of the aromatic ring. All attempts using a range of chemical analytical techniques to identify any impurity in the samples of **4** and **5** proved unsuccessful. In addition, HPLC analysis of incubations of **5** with the components of the co-crystallisations either on their own or in combination, including the presence of the protein, indicated no apparent degradation of **5**. This electron density remains unassigned.

An interesting variation in the degree of asymmetric induction in the quinolone hydroxylation reaction was also observed as a function of structure, although in all cases the absolute configuration of the resulting analogue was the same [(*S*)-(−)]. Quinolones **15–17** all reacted with (−)-[(8,8-dichlorocamphoryl)sulfonyl]oxaziridine (**18**)[11] under optimised conditions to give the desired analogues **5–7** respectively in good yield and high enantiomeric excess (ee 86–90%) in line with our report[9] on the synthesis of **1** (Scheme 1, column 8). As expected,[9] the ee of the asymmetric hydroxylation reaction for these substrates was reduced significantly when the dihydro-oxaziridine **19** was used instead of **18** (Scheme 1, column 9). Bach *et al.*[12] have reported a detailed computational analysis of the transition state involved in lithium enolate hydroxylation reactions using an oxaziridine. The steric bulk associated with the oxygen-bound lithium counter ion was identified as a major factor in determining the observed absolute stereochemical outcome of these reactions. Interestingly in our hands, ^{7}Li NMR analysis of the species formed on addition of 1.2 equivalents of LiHMDS to a dry THF solution of quinolones **15**, **16** and **17** at −78 °C showed the presence of a single peak at δ 0.69, 0.69 and 0.68 ppm respectively (Fig. 3b–d). LiHMDS in dry THF gave a single peak at δ 0.33 (Fig. 3e).

In contrast, oxidation of quinolone **13** with **18** (Scheme 1) gave **4** in good yield but with a significantly lower ee (65%) than for the other analogues as judged by chiral HPLC analysis of the crude reaction mixture. When **13** was treated with LiHMDS and the reaction analysed by ^{7}Li NMR, one major peak was observed with a chemical shift of 0.18 ppm (Fig. 3a). A second minor peak was also observed. It is tempting to speculate that the observed difference in ee for the hydroxylation of the enolate of **13** (*cf*. the enolates of **15**, **16**, **17** and **14**[9]) results from the formation of an alternative transition state in which the lithium atom is coordinated to the nitrogen atom rather than the oxygen. The formation of the O–Li enolate could be disfavored due to the potential steric clash with the C5-methyl-substituent in **13** (R^1 = Me, Scheme 1). Differences in the aggregation states of lithium enolates may also account for the observed differences in both the ^{7}Li NMR spectra and the differential reactivity.[13] To the best of our knowledge, these studies in the blebbistatin system are the first time that the enolate of a quinolone system, which can potentially

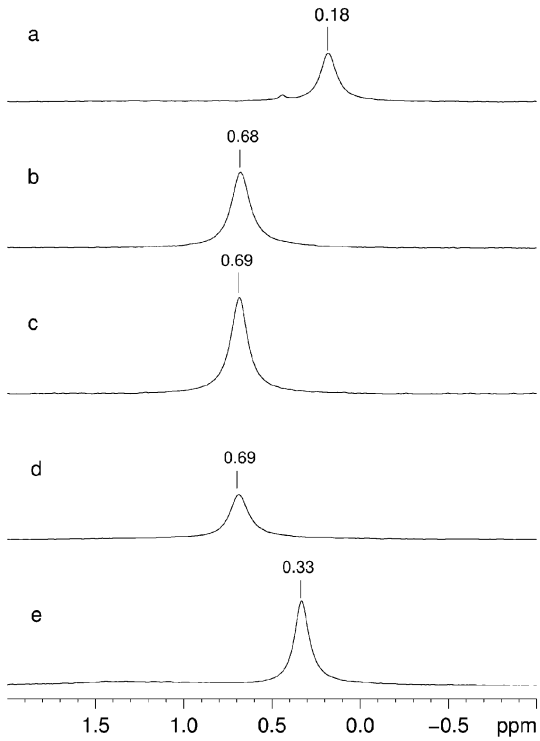

Fig. 3 ^{7}Li NMR spectra for the different enolate anions. Conditions: −78 °C, THF, LiHMDS. A capillary containing acetone-d^{6} was used as a lock signal in each case. ^{7}Li chemical shifts are given with respect to 0.1 M solution of Li_2SO_4 as an external standard, with a $\delta = 0$ ppm in H_2O. (a) **13**, (b) **15**, (c) **16**, (d) **17**, (e) LiHMDS.

have the lithium atom coordinated to the oxygen or the nitrogen in the transition state for hydroxylation, has been used in the Davis reaction. Our results suggest that this may prove an interesting system for more detailed study including computational analysis.

Highly optically enriched samples of the analogues **4**–**7** (ee >99%) were obtained by a single recrystallisation from acetonitrile of the product from the Davis hydroxylation reaction in line with our studies on **1**.[9] With the analogues of **1** in hand, assays against two myosin fragments (skeletal S1 and S1dC) were used to identify structure–activity relationships.

Biological activity against skeletal S1 and S1dC myosin fragments

A previous report has described the inhibition of a class II myosin (S1dC) obtained from the slime mould *Dictyostelium discoideum* by (*S*)-(−)-blebbistatin (**1**).[5] Using an analogous approach to that described previously,[5] **1** (as expected) and 3 of the 4 analogues were shown to inhibit completely the ATPase activity of S1dC at a final concentration of 50 μM (ESI, Table S1†). However, a clear outlier was also identified with analogue **6** (for structure see Fig. 1) being significantly less potent (65% residual S1dC ATPase activity remaining under analogous assay conditions†). This trend for reduced potency of **6** compared to the other analogues was mirrored in studies carried out using rabbit skeletal myosin S1 fragment at a final inhibitor concentration of both 5 μM and 50 μM, although at the higher concentration **6** was observed to reduce the ATPase activity by >70%.†

Co-crystal structures with S1dC

In order to correlate the observed biological activities of the blebbistatin analogues against S1dC with their interactions with this myosin at the molecular level, we have performed co-crystallisation experiments with each of the analogues **4**–**7** and the MgADP–vanadate complex of *Dictyostelium discoideum* myosin II. The complexes with **4**, **5**, **6** and **7** were solved by molecular replacement to resolutions of 2.0 Å, 2.2 Å, 2.15 Å and 2.1 Å respectively, using the (*S*)-(−)blebbistatin (**1**)–myosin structure as the starting model.† With the exception of analogue **6**, the electron density observed for each compound allowed all atoms to be modelled into the 50 kDa cleft where their position and orientation is nearly identical to that of **1** (Fig. 2). Alignment of the myosin complexes formed with **4**, **5** and **7** onto the model of **1** shows that these analogues do not significantly alter the conformation of residues comprising the binding pocket relative to those of the blebbistatin-bound form. In addition, their interaction did not produce any significant conformational changes in the overall protein structure as the α-carbons of all complexes superimpose on the original (*S*)-(−)-blebbistatin (**1**) model with a root mean square deviation of less than 0.2 Å.† Furthermore, their hydrogen bonding interactions with myosin and the surrounding water activity within the 50 kDa cleft were identical to the structure of **1**.

Unlike the other analogues, the electron density observed in the co-crystallisation experiment using **6** was not sufficiently unambiguous to allow this analogue to be modelled into the blebbistatin binding pocket. The absence of **6** in the model is further justified by the characteristics of Leu262 and Tyr634. In the (*S*)-(−)-blebbistatin (**1**)-bound form, the side chains of these residues move considerably in order to accommodate the *N*-phenyl ring and tricyclic core. Such movements are not observed for the co-crystallisation experiment with **6**. The lack of occupancy for **6** can be rationalised based on the observation that the methyl-substituent at position 8 (Scheme 1 for numbering) would create an unacceptably close hydrophobic contact (< 2.5 Å) with Tyr634, whose side chain has already been shown to move ∼3.6 Å to accommodate **1** (even in the absence of the 8-methyl-substituent, Fig. 2d). Therefore, it is apparent that **6** does not have suitable structural characteristics for formation of a stable interaction with *Dictyostelium discoideum* myosin II.

When taken together with the measured inhibitory effects of the analogues against both rabbit skeletal myosin S1 and *Dictyostelium* myosin II S1dC fragments, the crystallographic data strongly support the view that the inhibitor binding mode that is observed by X-ray crystallography is of relevance to the mechanism of myosin II inhibition by **1** and its analogues. Indeed, a methyl group at the C5, C6 or C7-position of the tricyclic core (in **4**, **1** or **5** respectively), or the absence of this group altogether as in **7**, allows the compound to remain structurally compatible with the 50 kDa cleft of *Dictyostelium discoideum* myosin II and able to trap the protein in the metastable state of the contractile cycle, inhibiting myosin activity. Methyl incorporation at the 8-position, on the other hand, is incompatible with adoption of a functional binding mode and thus does not have a robust inhibitory effect on *Dictyostelium discoideum* myosin II. Moreover, the conservation of residue identity or similarity in the equivalent pocket of skeletal myosin S1 fragment provides the basis for the parallels observed in the inhibitory effect of the analogues on both proteins.[8]

The design of focused libraries based on (*S*)-(−)blebbistatin (1)

The synthetic approach currently adopted for preparing analogues of **1** (Scheme 1) requires that the methyl-containing aromatic ring is incorporated from the outset of the synthesis. Our analysis of analogues with variations in this ring in complex with S1dC has shown that small substituents on the C5, C6 and C7-positions are well tolerated (Fig. 2 and Scheme 1 for numbering system). By varying these substituents to create more diverse analogues it may prove possible to prepare analogues that have either improved affinity for the subset of myosin II isoforms that **1** inhibits or that are specific for different myosin subtypes. We have further analysed the co-crystal structures reported here with the aim of designing inhibitors with increased affinity. Tyr261 forms a π–π stacking interaction with the aromatic ring of the core fragment of **1** which appears to contribute significantly to the binding affinity (Fig. 2 and 4). Interactive modelling of potential analogues of **1** using the MAB force field as implemented in Moloc[14] revealed that this interaction could be improved by extending the aromatic ring system, for example, by incorporating an additional thiophene ring to give analogue **20** (Fig. 4). Based on the modelling, both a ring joining the C6 and C7 positions and a ring joining the C5 and C6 positions could be accommodated in the binding pocket. However, the fact that the selectivity of the asymmetric hydroxylation reaction was shown here to decrease in the presence of a C5-substituent suggests that future studies should focus on the preparation of analogues such as **20** with substitutents at the C6 and C7 positions only.

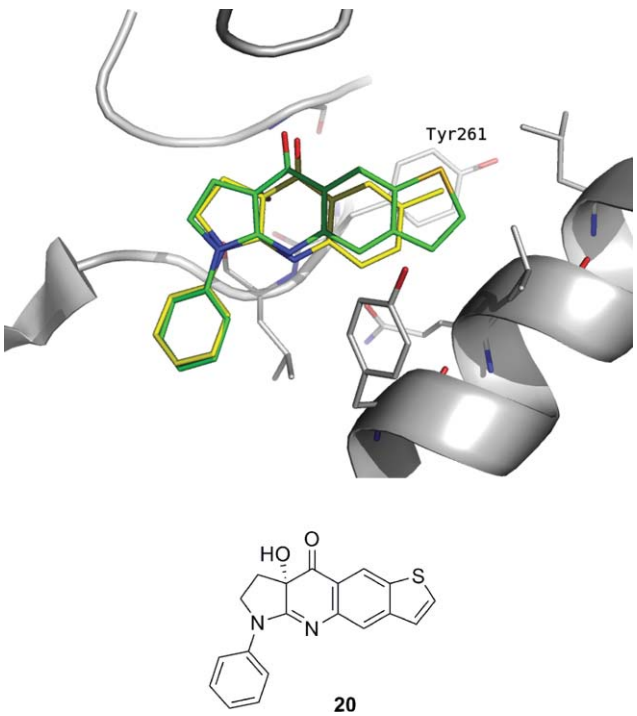

Fig. 4 Modeled binding mode of an analogue of **1** with an extended aromatic ring system (carbon atoms coloured in green) superimposed onto the crystallographically determined binding mode of **1** (carbon atoms coloured in yellow). The extended ring system is designed to increase the π–π stacking interaction with Tyr261.

Conclusion

The small molecule (*S*)-(−)-blebbistatin (**1**) has been quickly adopted by the myosin research community as a means of moving forward our understanding of the role of myosins in complex biological processes. Through modification of the chemical structure of **1** there is considerable potential to develop a second generation of tools that are either more potent than **1** or exhibit a modified selectivity across the myosin superfamily. Here, a combination of studies in chemistry and biology have enabled us to develop an initial view of what structural modifications can and cannot be accommodated in the methyl-substituted aromatic ring of **1**. In general, this region of **1** is relatively tolerant to changes in the position of the methyl-substituent with the exception of its incorporation at the 8-position. X-Ray crystallographic studies using *Dictyostelium discoideum* myosin II (S1dC) have led to a clear rationalisation of the observed variations in biological activity with a steric interaction between the 8-methyl-substituent and Tyr634 being responsible for the observed significant reduction in activity associated with analogue **6**. Our observed correlation between the ATPase activity and ability to adopt the same binding mode as **1** across a series of analogues further strengthens the view that this is the biologically relevant binding mode.

During the course of our synthesis of these analogues of **1**, it became clear that whilst acceptable from a biological activity perspective, the incorporation of a substituent in the 5-position (as in **4**) results in a reduction in the efficiency of the key asymmetric hydroxylation reaction. We therefore concluded that the incorporation of substituents at the 6- and 7-positions should be focused on in future attempts to optimise the potency of **1** against this particular myosin subclass. A preliminary computational assessment of this has been included that helps to define future synthetic targets.

Experimental

Unless otherwise noted, starting materials and reagents were obtained from commercial suppliers and were used without further purification. PE 40–60 refers to the fraction of light petroleum ether boiling in the range 40–60 °C. Melting points were recorded using an Electrothermal 9100 capillary melting point apparatus. Values are quoted to the nearest 0.5 °C. IR spectra were measured on a Perkin-Elmer Paragon 1000 FT-IR spectrometer. ^{1}H and ^{13}C NMR spectra were measured on a Brüker Advance 300/500 instrument. *J* values are quoted in Hz. Chemical shifts are calibrated with reference to the residual proton and carbon resonances of the solvent ($CDCl_3$: $\delta H = 7.26$, $\delta C = 77.0$ ppm). Low and high-resolution mass spectral analyses were recorded using ES operating in positive or negative ion mode.

General procedure for the synthesis of amidines 8, 10–12

Phosphorus oxychloride (1.0 equiv) was added dropwise to a solution of 1-phenyl-2-pyrrolidinone (1.1 equiv.) in dry dichloromethane (5.0–10 mL) and the reaction mixture was stirred for 3 h at room temperature. A solution of the corresponding anthranilate (1.0 equiv) in dry dichloromethane (15–25 mL) was then added and the mixture refluxed for 16–72 h, cooled and concentrated *in vacuo*. The resulting solid was dissolved in

aqueous hydrochloric acid (0.30 M, 100 mL) and extracted with dichloromethane (3 × 100 mL). The aqueous phase was basified with aqueous sodium hydroxide solution (2.0 M, pH adjusted to 8) and extracted with ethyl acetate (3 × 100 mL). The first organic extracts were concentrated *in vacuo* and the resulting solid was carried through the above procedure three more times. All ethyl acetate extracts were combined, dried ($MgSO_4$) and concentrated *in vacuo* to give the desired amidine.

Methyl 6-methyl-2-(1′-phenylpyrrolidin-2′-ylideneamino)benzoate (8). White solid (0.32 g, 1.0 mmol, 28%), mp 97–98 °C. IR (Nujol): ν_{max} = 1718 (s) (C=O), 1647 (s) (C=N), 1587 (m), 761 (m) (Ar-H), 722 (m), 692 cm^{-1} (m). ^1H NMR (300 MHz, $CDCl_3$): δ = 1.96–2.08 (m, 2 H, 4′-*H*), 2.34 (s, 3 H, CH_3), 2.59 (t, ^3J = 7.8, 2 H, 3′-*H*), 3.79–3.86 (m, 5 H, 5′-*H*, OCH_3), 6.62–6.68 (m, 1 H, 5-*H*), 6.82–6.88 (m, 1 H, 3-*H*), 7.03–7.10 (m, 1 H, 4″-*H*), 7.14–7.21 (m, 1 H, 4-*H*), 7.31–7.39 (m, 2 H, 3″-*H*), 7.76–7.83 ppm (m, 2 H, 2″-*H*). ^{13}C NMR (75.5 MHz, $CDCl_3$): δ = 19.4 (CH_3), 19.8 (CH_2), 29.3 (CH_2), 50.5 (CH_2), 51.8 (OCH_3), 118.7 (CH), 120.0 (C), 123.0 (C), 123.7 (CH), 127.5 (C), 128.5 (CH), 129.7 (CH), 135.3 (C), 141.2 (C), 149.4 (C), 161.0 (C), 170.2 ppm (C). LRMS (ES^+) *m*/*z* (%): 309 (100) $[M + H]^+$. HRMS (ES^+): *m*/*z* calcd for $C_{19}H_{21}N_2O_2$ $[M + H]^+$: 309.1603; found: 309.1610.

Methyl 4-methyl-2-(1′-phenylpyrrolidin-2′-ylideneamino)benzoate (10). Waxy solid (0.66 g, 2.1 mmol, 24%). IR (Nujol): ν_{max} = 1690 (s) (C=O), 1602 (s) (C=N), 1529 (m), 779 (m), 750 (m) (Ar-H), 693 cm^{-1} (m). ^1H NMR (300 MHz, $CDCl_3$): δ = 1.97–2.08 [m, 2 H, 4′-*H*], 2.32 (br s, 3 H, CH_3), 2.47 (t, ^3J = 7.8, 2 H, 3′-*H*), 3.80 (s, 3 H, OCH_3), 3.86 (t, ^3J = 6.9, 2 H, 5′-*H*), 6.66 (br s, 1 H, 3-*H*), 6.83 (ddq, ^3J = 8.0, ^4J = 1.6, ^4J = 0.5, 1 H, 5-*H*), 7.02–7.09 (m, 1 H, 4″-*H*), 7.31–7.40 (m, 2 H, 3″-*H*), 7.80 (d, ^3J = 8.0, 1 H, 6-*H*), 7.82–7.87 ppm (m, 2 H, 2″-*H*). ^{13}C NMR (75.5 MHz, $CDCl_3$): δ = 19.5 (CH_2), 21.3 (CH_3), 29.0 (CH_2), 50.3 (CH_2), 51.4 (OCH_3), 118.9 (C), 120.0 (CH), 122.4 (CH), 122.7 (CH), 123.5 (CH), 128.3 (CH), 130.9 (CH), 141.2 (C), 143.2 (C), 153.1 (C), 159.2 (C), 167.2 ppm (C). LRMS (ES^+) *m*/*z* (%): 309 (100) $[M + H]^+$, 277 (24) $[M\text{-}MeOH]^+$. HRMS (ES^+): *m*/*z* calcd for $C_{19}H_{21}N_2O_2$ $[M + H]^+$: 309.1603; found: 309.1597.

Methyl 3-methyl-2-(1-phenylpyrrolidin-2-ylideneamino)benzoate (11). White crystalline solid after 72 h reflux (0.65 g, 2.1 mmol, 52%), mp 95–96 °C. IR (Nujol): ν_{max} = 1720 (s) (C=O), 1654 (s) (C=N), 1587 (m), 747 (m) (Ar-H), 722 cm^{-1} (m). ^1H NMR (300 MHz, $CDCl_3$): δ = 1.98–2.10 (m, 2 H, 4′-*H*), 2.10–2.25 (m, 4 H, 3′-*H*, CH_3), 2.52–2.67 (m, 1 H, 3′-*H*), 3.78 (s, 3 H, OCH_3), 3.89 (t, ^3J = 6.8, 2 H, 5′-*H*), 6.91–6.97 (m, 1 H, 5-*H*), 7.07 (m, 1 H, 4″-*H*), 7.29–7.34 (m, 1 H, 4-*H*), 7.34–7.41 (m, 2 H, 3″-*H*), 7.70 (m, 1 H, 6-*H*), 7.83–7.90 ppm (m, 2 H, 2″-*H*). ^{13}C NMR (75.5 MHz, $CDCl_3$): δ = 18.2 (CH_3), 19.3 (CH_2), 29.4 (CH_2), 50.2 (CH_2), 51.3 (OCH_3), 119.8 (CH), 120.9 (CH), 121.2 (C), 122.4 (CH), 128.1 (CH), 128.2 (CH), 130.0 (C), 133.4 (CH), 141.3 (C), 151.3 (C), 158.9 (C), 167.5 ppm (C). IR (Nujol): ν_{max} = 1720 (s) (C=O), 1654 (s) (C=N), 1587 (m), 747 (m) (Ar-H), 722 cm^{-1} (m). LRMS (ES^+) *m*/*z* (%): 309 (100) $[M + H]^+$. HRMS (ES^+): *m*/*z* calcd for $C_{19}H_{21}N_2O_2$ $[M + H]^+$: 309.1603; found: 309.1610.

Methyl 2-(1-phenylpyrrolidin-2-ylideneamino)benzoate (12). White crystalline solid, (0.40 g, 1.4 mmol, 26%), mp 127–128 °C. IR (Nujol): ν_{max} = 1721 (s) (C=O), 1654 (s) (C=N), 1591 (m), 756 (m) (Ar-H), 692 cm^{-1} (m). ^1H NMR (300 MHz, $CDCl_3$): δ = 1.99–2.11 (m, 2 H, 4′-*H*), 2.48 (t, ^3J = 7.9, 2 H, 3′-*H*), 3.83 (s, 3 H, OCH_3), 3.88 (t, ^3J = 6.9, 2 H, 5′-*H*), 6.82 (dd, ^3J = 8.0, ^4J = 1.0, 1 H, 3-*H*), 6.98–7.10 (m, 2 H, 4″, 5-*H*), 7.31–7.41 (m, 3 H, 3″, 4-*H*), 7.77–7.89 ppm (m, 3 H, 2″, 6-*H*). ^{13}C NMR (75.5 MHz, $CDCl_3$): δ = 19.6 (CH_2), 29.1 (CH_2), 50.5 (CH_2), 51.6 (OCH_3), 120.2 (CH), 121.5 (CH), 122.1 (C), 122.9 (CH), 123.1 (CH), 128.4 (CH), 130.7 (CH), 132.5 (CH), 141.2 (C), 153.0 (C), 159.4 (C), 167.5 ppm (C). LRMS (ES^+) *m*/*z* (%): 295 (100) $[M + H]^+$, 263 (22) $[M\text{-}OMe]^+$. HRMS (ES^+): *m*/*z* calcd for $C_{18}H_{19}N_2O_2$ $[M + H]^+$: 295.1447; found: 295.1449.

General procedure for the synthesis of quinolones 13, 15–17

A solution of the corresponding amidine (1.0 equiv.) in anhydrous THF (50 mL) was cooled to −78 °C and stirred for 15 min. Lithium bis(trimethylsilyl)amide (1.0 M in THF, 3.0 equiv.) was added dropwise to the reaction mixture, which was warmed to 0 °C over 3 h or room temperature over 12 h and quenched with saturated aqueous ammonium chloride (5.0 mL). Further saturated aqueous ammonium chloride (150 mL) was added. The aqueous phase was extracted with dichloromethane (3 × 100 mL) and the combined organic extracts dried ($MgSO_4$) and concentrated *in vacuo*. Purification by flash column chromatography on silica gel eluting with (50–100% ethyl acetate–PE 40–60) gave the desired compound.

5-Methyl-1-phenyl-2,3,4,9-tetrahydro-1*H*-pyrrolo[2,3-*b*]quinolin-4-one (13). Off-white solid (0.044 g, 0.16 mmol, 84%), mp 240–241 °C. IR (Nujol): ν_{max} = 1614 (m), 1570 (s), 1310 (s), 754 (m) (Ar-H), 722 cm^{-1}(m). ^1H NMR (300 MHz, d_8-THF): δ = 2.85 (s, 3 H, CH_3), 3.16 (t, ^3J = 8.3, 2 H, 3-*H*), 4.02 (t, ^3J = 8.3, 2 H, 2-*H*), 6.85–6.90 (m, 1 H, 6-*H*), 6.91–6.97 (m, 1 H, 4′-*H*), 7.21 (dd, ^3J = 8.2, ^3J = 7.2, 1 H, 7-*H*), 7.26–7.34 (m, 2 H, 3′-*H*), 7.41–7.46 (m, 1 H, 8-*H*), 7.93–8.00 ppm (m, 2 H, 2′-*H*). ^{13}C NMR (75.5 MHz, d_8-THF)¶: δ = 23.0 (CH_2), 24.4 (CH_3), 49.9 (CH_2), 106.6 (C), 118.7 (CH), 118.9 (C), 121.9 (CH), 124.5 (CH), 125.6 (CH), 128.4 (CH), 129.0 (CH), 135.7 (C), 143.3 (C), 149.0 (C), 156.1 (C), 158.0 ppm (C). IR (Nujol): ν_{max} = 1614 (m), 1570 (s), 1310 (s), 754 (m) (Ar-H), 722 cm^{-1}(m). LRMS (ES^+), *m*/*z* (%): 277 (100) $[M + H]^+$. HRMS (ES^+): *m*/*z* calcd for $C_{18}H_{17}N_2O$ $[M + H]^+$: 277.1341; found: 277.1336.

7-Methyl-1-phenyl-2,3,4,9-tetrahydro-1*H*-pyrrolo[2,3-*b*]quinolin-4-one (15). Off-white solid (0.51 g, 1.8 mmol, 95%), mp 186–187 °C. IR (Nujol): ν_{max} = 1630 (m), 1578 (s), 1308 (w), 750 (m) (Ar-H), 722 (m), 688 cm^{-1}(w). ^1H NMR (500 MHz, d_8-THF): δ = 2.41 (s, 3 H, CH_3), 3.16 (t, ^3J = 8.2, 2 H, 3-*H*), 4.01 (t, ^3J = 8.2, 2 H, 2-*H*), 6.90–6.97 (m, 1 H, 4′-*H*), 7.00 (m, 1 H, 6-*H*), 7.25–7.34 (m, 2 H, 3′-*H*), 7.41 (br s, 1 H, 8-*H*), 7.92 (d, ^3J = 8.2, 1 H, 5-*H*), 7.96–8.05 ppm (m, 2 H, 2′-*H*). ^{13}C NMR (75.5 MHz, d_8-THF)¶: δ = 21.5 (CH_3), 22.8 (CH_2), 49.8 (CH_2), 105.5 (C), 117.7 (C), 118.8 (CH), 121.8 (CH), 122.2 (CH), 124.0 (CH), 128.0 (CH), 129.0 (CH), 139.0 (C), 143.3 (C), 144.0 (C), 149.2 (C), 160.6 ppm (C). LRMS (CI^+) *m*/*z* (%): 305 (11), 277 (99) $[M + H]^+$. HRMS (CI^+): *m*/*z* calcd for $C_{18}H_{17}N_2O$ $[M + H]^+$: 277.1341; found: 277.1342.

8-Methyl-1-phenyl-2,3,4,9-tetrahydro-1*H*-pyrrolo[2,3-*b*]quinolin-4-one (16). Off-white solid (0.42 g, 1.5 mmol, 95%), mp

¶ The assignment of ^{13}C signals was made by using Pendant, HMBC and HSQC NMR analysis.

231–232 °C. IR (Nujol): $\nu_{max} = 1566$ (s), 1539 (m), 1307 (s), 1075 (w), 750 (m) (Ar-H), 722 (m), 693 cm^{-1}(m). ^1H NMR (500 MHz, d_8-THF): $\delta = 2.65$ (s, 3 H, CH_3), 3.16 (t, $^3J = 8.1$, 2 H, 3-*H*), 4.07 (t, $^3J = 8.1$, 2 H, 2-*H*), 6.89–6.96 (m, 1 H, 4′-*H*), 7.05 (dd, $^3J = 8.1$, $^3J = 7.0$, 1 H, 6-*H*), 7.27–7.36 (m, 3 H, 3′-*H*,7-*H*), 7.84 (br dd, $^3J = 8.1$, $^4J = 0.8$, 1 H, 5-*H*), 8.12–8.19 ppm (m, 2 H, 2′-*H*). ^{13}C NMR (125.7 MHz, d_8-THF)¶: $\delta = 18.8$ (CH_3), 22.4 (CH_2), 48.8 (CH_2), 106.1 (C), 117.7 (CH), 119.2 (C), 119.6 (CH), 121.1 (CH), 121.6 (CH), 128.8 (CH), 129.4 (CH), 134.3 (C), 143.5 (C), 148.7 (C), 155.2 (C), 160.0 ppm (C). LRMS (ES^+) *m/z* (%): 277 (100) $[M + H]^+$. HRMS (ES^+): *m/z* calcd for $C_{18}H_{17}N_2O$ $[M + H]^+$: 277.1341; found: 277.1336.

1-Phenyl-2,3,4,9-tetrahydro-1*H*-pyrrolo[2,3-*b*]quinolin-4-one (17). Off-white solid (0.42 g, 1.6 mmol, 95%), mp 189–190 °C. IR (Nujol): $\nu_{max} = 1630$ (s), 1575 (s), 1297 (w), 756 (m) (Ar-H), 722 (m), 695 cm^{-1} (m). ^1H NMR (300 MHz, d_8-THF): $\delta = 3.19$ (t, $^3J = 8.2$, 2 H, 3-*H*), 4.07 (t, $^3J = 8.2$, 2 H, 2-*H*), 6.91–6.98 (m, 1 H, 4′-*H*), 7.11–7.18 (m, 1 H, 6-*H*), 7.27–7.34 (m, 2 H, 3′-*H*), 7.36–7.43 (m, 1 H, 7-*H*), 7.58–7.64 (m, 1 H, 8-*H*), 8.00 (dd, $^3J = 8.2$, $^4J = 1.3$, 1 H, 5-*H*), 8.02–8.08 ppm (m, 2 H, 2′-*H*). ^{13}C NMR (75.5 MHz, d_8-THF)¶: $\delta = 22.6$ (CH_2), 49.5 (CH_2), 106.4 (C), 118.6 (CH), 119.6 (C), 121.8 (CH), 122.0 (CH × 2), 126.6 (CH), 128.9 (CH × 2), 143.3 (C), 148.4 (C), 157.7 (C), 159.5 ppm (C). LRMS (ES^+) *m/z* (%): 263 (100) $[M + H]^+$. HRMS (ES^+): *m/z* calcd for $C_{17}H_{15}N_2O$ $[M + H]^+$: 263.1184; found: 263.1180.

General procedure for the synthesis of analogues 4–7

A solution of the corresponding quinolone (1.0 equiv.) in dry THF (10–28 mL) was added dropwise to lithium bis(trimethylsilyl)amide (1.0 M in THF, 1.2 equiv.) in dry THF (2.0–5.0 mL) at −78 °C under argon. The reaction was stirred for 30 min at −78 °C and a solution of **18** (2.4 equiv.) (or **19**) in dry THF (4–10 mL) was added *via* cannula. After 16 h at −10 °C saturated aqueous ammonium iodide (5.0 mL, 10 equiv) and diethyl ether (5.0 mL) were added and the reaction mixture gradually warmed to room temperature. Saturated aqueous sodium thiosulfate (5–15 mL) was then added and the reaction mixture extracted with diethyl ether (2 × 10 mL). The combined organic extracts were dried ($MgSO_4$) and concentrated *in vacuo.* The solid was partitioned between dichloromethane (100 mL) and aqueous hydrochloric acid solution (0.30 M, 100 mL). The aqueous phase was washed with dichloromethane (3 × 100 mL), basified with aqueous sodium hydroxide solution (2.0 M, pH adjusted to 8) and extracted with ethyl acetate (2 × 100 mL). The organic extracts were dried ($MgSO_4$) and concentrated *in vacuo* to give the desired compound.

***S*-3a-Hydroxy-5-methyl-1-phenyl-2,3,3a,4-tetrahydro-1*H*-pyrrolo[2,3-*b*]quinolin-4-one (4).** Bright yellow solid (0.020 g, 0.070 mmol, 87%), ee 64% as determined by chiral-phase HPLC analysis (Daicel Chiralpak AD, acetonitrile–water 50 : 50, flow rate 0.8 mL min^{-1}, $\lambda = 254$ nm, major enantiomer: $t_R = 6.05$ min, and minor enantiomer: $t_R = 8.02$ min), mp 227–228 °C, $[\alpha]_D^{25} = -310$ ($c = 0.1$ in dichloromethane). IR (Nujol): $\nu_{max} = 1686$ (m), 1618 (m), 1590 (m), 1313 (w), 1262 (w), 723 cm^{-1}(m) (Ar-H). ^1H NMR (300 MHz, d_8-THF): $\delta = 2.19$–2.37 (m, 2 H, 3-*H*), 2.53 (s, 3 H, CH_3), 3.90–3.98 (m, 1 H, 2-*H*), 4.11 (dt, $^2J = 9.6$, $^3J = 6.4$, 1 H, 2-*H*), 6.82 (m, 1 H, 6-*H*), 7.02–7.11 (m, 2 H, 4′,7-*H*), 7.25–7.29 (m, 1 H, 8-*H*), 7.30–7.38 (m, 2 H, 3′-*H*), 8.08–8.14 ppm (m, 2 H, 2′-*H*). ^{13}C NMR (75.5 MHz, d_8-THF): $\delta = 21.5$ (CH_3), 29.6 (CH_2), 48.4 (CH_2), 75.0 (C), 120.1 (CH), 121.1 (C), 123.9 (CH), 125.2 (CH), 127.0 (CH), 129.04 (CH), 134.3 (CH), 141.4 (C), 142.0 (C), 153.3 (C), 166.0 (C), 197.0 ppm (C). LRMS (ES^+): *m/z* (%): 293 (100) $[M + H]^+$. HRMS (ES^+): *m/z* calcd for $C_{18}H_{17}N_2O_2$ $[M + H]^+$: 293.1290; found: 293.1288. Anal. calcd for $C_{18}H_{16}N_2O_2$: C, 73.95; H, 5.52; N, 9.58; found: C, 73.75; H, 5.54; N, 9.67. An analytical sample of **4** was prepared by recrystallisation from acetonitrile; $[\alpha]_D^{25} = -450$ ($c = 0.07$ in dichloromethane). Chiral HPLC analysis showed that after a single recrystallisation **4** was prepared with an ee of 98.9%. When this reaction was carried out using **19** instead of **18**, the ee was 17%.

***S*-3a-Hydroxy-7-methyl-1-phenyl-2,3,3a,4-tetrahydro-1*H*-pyrrolo[2,3-*b*]quinolin-4-one (5).** Bright yellow solid (0.045 g, 0.15 mmol, 83%), ee 90% as determined by chiral-phase HPLC analysis (Daicel Chiralpak AD, acetonitrile–water 50 : 50, flow rate 1.0 mL min^{-1}, $\lambda = 254$ nm, major enantiomer: $t_R = 9.39$ min, and minor enantiomer: $t_R = 12.42$ min), mp 223–224 °C, $[\alpha]_D^{25} = -354$ ($c = 0.1$ in dichloromethane). IR (Nujol): $\nu_{max} = 1664$ (m), 1593 (m), 1300 (w), 1264 (w), 752 (m) (Ar-H), 722 cm^{-1}(w). ^1H NMR (300 MHz, d_8-THF): $\delta = 2.16$–2.32 (m, 2 H, 3-*H*), 2.33 (s, 3 H, CH_3), 3.89–3.97 (m, 1 H, 2-*H*), 4.12 (dt, $^2J = 9.7$, $^3J = 6.2$, 1 H, 2-*H*), 6.84 (m, 1 H, 6-*H*), 7.05–7.10 (m, 2 H, 4′,8-*H*), 7.30–7.38 (m, 2 H, 3′-*H*), 7.66 (d, $^3J = 7.8$, 1 H, 5-*H*), 8.10–8.16 ppm (m, 2 H, Ar-2′-*H*). ^{13}C NMR (75.5 MHz, d_8-THF): $\delta = 21.6$ (CH_3), 29.6 (CH_2), 48.3 (CH_2), 74.0 (C), 120.2 (CH), 120.5 (C), 123.9 (CH), 124.5 (CH), 127.2 (CH), 127.4 (CH), 129.0 (CH), 142.0 (C), 146.7 (C), 152.7 (C), 167.0 (C), 194.3 ppm (C). LRMS (ES^+) *m/z* (%): 293 (100) $[M + H]^+$. HRMS (ES^+): *m/z* calcd for $C_{18}H_{17}N_2O_2$ $[M + H]^+$: 293.1290; found: 293.1296. Anal. calcd for $C_{18}H_{16}N_2O_2$: C, 73.95; H, 5.52; N, 9.58; found: C, 73.90; H, 5.56; N, 9.69. An analytical sample of **5** was prepared by recrystallisation from acetonitrile; $[\alpha]_D^{25} = -450$ ($c = 0.1$ in dichloromethane). Chiral HPLC analysis showed that after a single recrystallisation **5** was prepared with an ee of >99%. When this reaction was carried out using **19** instead of **18**, the ee was 28%.

***S*-3a-Hydroxy-8-methyl-1-phenyl-2,3,3a,4-tetrahydro-1*H*-pyrrolo[2,3-*b*]quinolin-4-one (6).** Bright yellow solid (0.13 g, 0.45 mmol, 63%), ee 86% as determined by chiral-phase HPLC analysis (Daicel Chiralpak AD, acetonitrile–water 50 : 50, flow rate 0.8 mL min^{-1}, $\lambda = 254$ nm, major enantiomer: $t_R = 16.67$ min, and minor enantiomer: $t_R = 52.30$ min), mp 214–215 °C, $[\alpha]_D^{25} = -420$ ($c = 0.1$ in dichloromethane). IR (Nujol): $\nu_{max} = 3329$ (s), 1670 (s), 1618 (s), 1590 (s), 1297 (m), 754 cm^{-1} (m) (Ar-H). ^1H NMR (500 MHz, d_8-THF): $\delta = 2.21$–2.35 (m, 2 H, 3-*H*), 2.45 (s, 3 H, CH_3), 3.94–3.99 (m, 1 H, 2-*H*), 4.13 (dt, $^2J = 9.6$, $^3J = 6.0$, 1 H, 2-*H*), 6.90–6.94 (m, $^3J = 7.5$, 1 H, 6-*H*), 7.05–7.09 (m, 1 H, 4′-*H*), 7.33–7.39 (m, 3 H, 3′,7-*H*), 7.62–7.65 (m, 1 H, 5-*H*), 8.16–8.20 ppm (m, 2 H, 2′-*H*). ^{13}C NMR (125.7 MHz, d_8-THF): $\delta = 18.3$ (CH_3), 29.6 (CH_2), 48.1 (CH_2), 73.4 (C), 119.9 (CH), 122.0 (C), 123.1 (CH), 123.8 (CH), 124.9 (CH), 129.1 (CH), 134.3 (C), 136.9 (CH), 142.0 (C), 150.5 (C), 165.6 (C), 195.2 ppm (C). LRMS (ES^+) *m/z* (%): 293 (100) $[M + H]^+$. HRMS (ES^+): *m/z* calcd for $C_{18}H_{17}N_2O_2$ $[M + H]^+$: 293.1290; found: 293.1300. An analytical sample of **6** was prepared by recrystallisation from acetonitrile. Anal. calc'd for $C_{18}H_{16}N_2O_2$: C, 73.95; H, 5.52; N, 9.58; found: C, 73.62; H, 5.58; N, 9.60. Chiral HPLC analysis

showed that after a single recrystallisation, **6** was prepared with an ee of >99%. When this reaction was carried out using **19** instead of **18**, the ee was 40%.

***S*-3a-Hydroxy-1-phenyl-2,3,3a,4-tetrahydro-1*H*-pyrrolo[2,3-*b*]-quinolin-4-one (7).** Bright yellow solid (0.040 g, 0.15 mmol, 78%), ee 86% as determined by chiral-phase HPLC analysis (Daicel Chiralpak AD, acetonitrile–water 50 : 50, flow rate 0.9 mL min^{-1}, $\lambda = 254$ nm, major enantiomer: $t_R = 7.72$ min, and minor enantiomer: $t_R = 11.07$ min), mp 203–204 °C, $[\alpha]_D^{25} = -414$ ($c = 0.1$ in dichloromethane). ^{1}H NMR (300 MHz, $CDCl_3$): $\delta = 2.21$–2.34 (m, 1 H, 3-*H*), 2.41–2.50 (m, 1 H, 3-*H*), 3.83–3.92 (m, 1 H, 2 *H*), 4.03 (dt, $^2J = 9.8$, $^3J = 5.8$, 1 H, 2-*H*), 7.05 (dt, $^3J = 7.5$, $^4J = 1.1$, 1 H, 6-*H*), 7.16–7.23 (m, 2 H, 4′,8-*H*), 7.37–7.47 (m, 3 H, 3′,5-*H*), 7.83–7.87 (m, 1 H, 7-*H*), 7.88–7.93 ppm (m, 2 H, 2′-*H*). ^{13}C NMR (75.5 MHz, d_8-THF): $\delta = 29.6$ (CH_2), 48.3 (CH_2), 74.0 (C), 120.3 (CH), 122.44 (C), 123.5 (CH), 124.0 (CH), 127.0 (CH), 127.1 (CH), 129.0 (CH), 135.7 (CH), 141.9 (C), 152.6 (C), 166.7 (C), 194.8 ppm (C. IR (Nujol): $\nu_{max} = 1698$ (m), 1618 (m), 1593 (m), 1294 (w), 723 cm^{-1}(m) (Ar-H). LRMS (ES^+) *m*/*z* (%): 279 (100) $[M + H]^+$. HRMS (ES^+): *m*/*z* calcd for $C_{17}H_{15}N_2O_2$ $[M + H]^+$: 279.1134; found: 279.1141. Anal. calc'd for $C_{17}H_{14}N_2O_2$: C, 73.37; H, 5.07; N, 10.07; found: C, 73.26; H, 4.84; N, 10.28. An analytical sample of **7** was prepared by recrystallisation from acetonitrile; $[\alpha]_D^{25} = -460$ ($c = 0.1$ in dichloromethane. Chiral HPLC analysis showed that after a single recrystallisation, **7** was prepared with an ee of >99%. When this reaction was carried out using **19** instead of **18**, the ee was 55%.

General procedure for preparation and ^{7}Li NMR analysis of quinolone enolates

A solution of the quinolone (0.025 g, 0.090 mmol, 1.0 eq) in anhydrous THF (10 mL) was cooled to −78 °C and stirred for 5 min. Lithium bis(trimethylsilyl)amide (1.0 M in THF, 0.11 mL, 0.11 mmol, 1.2 equiv.) was then added to the reaction mixture, at −78 °C. An aliquot from the reaction mixture was transfer to an NMR tube, under an inert atmosphere, and analysed by ^{7}Li NMR (116.6 MHz), at −78 °C. A capillary containing acetone-d^6 was used as a lock signal in each case. ^{7}Li chemical shifts are given with respect to 0.1 M solution of Li_2SO_4 (as external standard, with a $\delta = 0$ ppm) in H_2O.

Procedures for crystallisation studies

A truncated version of *Dictyostelium* myosin II (S1dC) containing residues Asp2-Asn762 was used for all crystallisation experiments. The S1dC construct was cloned into a recombinant version of the pDXA vector (pDTEV2), which inserts a 6-His tag followed by an rTEV protease recognition site at the *N*-terminus of myosin. This construct was expressed and purified from *Dictyostelium discoideum* as previously described.[8,15] Co-crystallisation of this myosin with each of the blebbistatin analogues was achieved by addition of the analogue at a final concentration of 0.5 mM followed by one tenth of the volume of a 10X MgADP.Vi stock solution containing 10 mM $MgCl_2$, 20 mM ADP, and 30 mM sodium vanadate.[16] This mixture was incubated on ice in the dark for 1 h to allow the analogue and the nucleotide to form a stable complex with myosin. Crystals of these complexes were grown in the dark at 4 °C by vapor diffusion after mixing 5 μl of protein with an equal volume of well solution containing 100 mM MOPS (pH 7.0), 250 mM $MgCl_2$, 12% PEG 8000, 1 mM TCEP, and 2 mM Thymol. The protein/precipitant solutions for all analogue complexes were streak-seeded from preliminary crystals and grew to maximum dimensions within 2 to 3 weeks.

Data collection

Crystals were transferred from the original drop to a synthetic mother liquor containing 100 mM MOPS (pH 7.0), 225 mM $MgCl_2$, 2 mM thymol, 12% PEG 8000, 1X MgADP.Vi trapping solution, and 0.5 mM of each blebbistatin analogue. Prior to freezing in a stream of nitrogen gas, the crystals were gradually transferred from the synthetic mother liquor to a cryoprotectant solution of 100 mM MOPS (pH 7.0), 300 mM $MgCl_2$, 16% PEG 8000, 2 mM thymol, 1X MgADP.Vi trapping solution, 0.5 mM blebbistatin, and 25% ethylene glycol. X-Ray data were collected on a MAR-165 detector at the COM-CAT 32-ID beamline at the Advanced Photon Source in Argonne, Il with a wavelength of 1.0 Å. An oscillation range of 0.5° was used for all datasets. Diffraction data were integrated and scaled with the program HKL2000.[17]

Structure determination and refinement

The structures of each analogue–myosin complex were solved by molecular replacement using the Blebbistatin-MgADP.Vi-S1dC structure (PDB accession code 1YV3) as the starting model.[8] The structure models were subjected to manual and automated refinement using Coot and Refmac5, respectively.[18,19] Water molecules were added to the coordinate sets using Coot with subsequent manual verification.[18] Blebbistatin analogues were built into the electron density using the original blebbistatin coordinates as a starting model, followed by subsequent manual atom position refinement in Coot. Relevant X-ray data collection and refinement statistics are shown in the ESI, Table S1† in the supplementary material. Ramachandran statistics for the myosin polypeptide chain of each complex were determined using PROCHECK.[20] For the **5**–myosin complex 91.9% are in the most favored region, 7.7% additionally allowed, 0.3% generously allowed, and 0% disallowed. For the **4**–myosin complex 93.7% are in the most favored region, 6% additionally allowed, 0.3% generously allowed, and 0% disallowed. For the **7**–myosin complex 92.7% are in the most favored region, 7.1% additionally allowed, 0.2% generously allowed, and 0% disallowed. For the **6**–myosin complex 92.4% are in the most favored region, 7.3% additionally allowed, 0.3% generously allowed, and 0% disallowed.

Structure analysis and figure preparation

Structure alignments were performed with Superpose.[21] Figures were prepared using MacPymol.[22]

Acknowledgements

We would like to thank Dr Stephen Patterson for providing a sample of **8** and Laura Walker for assistance with the blebbistatin analogue–myosin co-crystallisations. We would also like to thank the following for funding: The Royal Society (NJW fellowship), EPSRC (CL-L PhD funding) and BBSRC (CPATL PhD

funding), NIH grant AR35186 (IR) and a Canadian Institutes of Health postdoctoral fellowship (64606 to JSA). The structural coordinates for the blebbistatin analogue-myosin complexes have been deposited in the RCSB under accession numbers 3BZ7 (**4**-myosin complex), 3BZ8 (**5**-myosin complex), and 3BZ9 (**7**-myosin complex).

References

1 A. F. Straight, A. Cheung, J. Limouze, I. Chen, N. J. Westwood, J. R. Sellers and T. J. Mitchison, *Science*, 2003, **299**(5613), 1743–1747. For recent examples of the use of blebbistatin to study cytokinesis see:; K. Miyauchi, Y. Yamamoto, T. Kosaka and H. Hosoya, *Biochem. Biophys. Res. Commun.*, 2006, **350**(3), 543–548; S. Matson, S. Markoulaki and T. Ducibella, *Biol. Reprod.*, 2006, **74**(1), 169–176; M. Kanada, A. Nagasaki and T.Q. P. Uyeda, *Mol. Biol. Cell*, 2005, **16**(8), 3865–3872; M. Guha, M. Zhou and Y. Wang, *Curr. Biol.*, 2005, **15**(8), 732–736; K. Murthy and P. Wadsworth, *Curr. Biol.*, 2005, **15**(8), 724–731; R. M. Pielak, V. A. Gaysinskaya and W. D. Cohen, *Dev. Biol.*, 2004, **269**(2), 421–432.

2 For recent examples of the use of blebbistatin to study cell migration see: N. Takizawa, R. Ikebe, M. Ikebe and E. J. Luna, *J. Cell Sci.*, 2007, **120**(21), 3792–3803; I. B. Barsoum and C. King-Smith, *Cell Motil. Cytoskeleton*, 2007, **64**(11), 868–879; R. Samaniego, L. Sanchez-Martin, A. Estecha and P. Sanchez-Mateos, *J. Cell Sci.*, 2007, **120**(20), 3534–3543; K. Yoshida and T. Soldati, *J. Cell Sci.*, 2006, **119**, 3833–44; J. Kolega, *Mol. Biol. Cell*, 2006, **17**, 4435–45; M. S. Duxbury, S. W. Ashley and E. E. Whang, *Biochem. Biophys. Res. Commun.*, 2004, **313**, 992–997.

3 For a recent review see: J. R. Peterson and T. J. Mitchison, *Chem. Biol.*, 2002, **9**(12), 1275–1285.

4 J. R. Sellers, *Biochim. Biophys. Acta*, 2000, **1496**, 3–22.

5 J. Limouze, A. F. Straight, T. Mitchison and J. R. Sellers, *J. Muscle Res. Cell Motil.*, 2004, **25**, 337–341.

6 B. Ramamurthy, C. M. Yengo, A. F. Straight, T. J. Mitchison and H. L. Sweeney, *Biochemistry*, 2004, **43**, 14832–14839.

7 M. Kovacs, J. Toth, C. Hetenyi, A. Malnasi-Csizmadia and J. R. Sellers, *J. Biol. Chem.*, 2004, **279**, 35557–35563.

8 J. S. Allingham, R. Smith and I. Rayment, *Nat. Struct. Mol. Biol.*, 2005, **12**, 378–9, and references therein.

9 C. Lucas-Lopez, S. Patterson, T. Blum, A. F. Straight, J. Toth, A. M. Z. Slawin, T. J. Mitchison, J. R. Sellers and N. J. Westwood, *Eur. J. Org. Chem.*, 2005, **9**, 1736–1740.

10 M. Cope, J. Whisstock, I. Rayment and J. Kendrick-Jones, *Structure*, 1996, **4**(8), 969–987.

11 F. A. Davis, M. C. Weismiller, C. K. Murphy, T. Reddy and B-C. Chen, *J. Org. Chem.*, 1992, **57**, 7274–7285.

12 R. D. Bach, J. L. Andres and F. A. Davis, *J. Org. Chem.*, 1992, **57**(2), 613–18.

13 A. J. McNeil, G. E. S. Toombes, S. M. Gruner, E. Lobkovsky, D. B. Collum, S. V. Chandramouli, B. J. Vanasse and T. A. Ayers, *J. Am. Chem. Soc.*, 2004, **126**, 16559–16568, and references therein.

14 P. R. Gerber, *J. Comput. Aided Mol. Des.*, 1998, **12**, 37–51.

15 A. J. Fisher, C. A. Smith, J. Thoden, R. Smith, K. Sutoh, H. M. Holden and I. Rayment, *Biochemistry*, 1995, **34**, 8960–8972.

16 C. A. Smith and I. Rayment, *Biochemistry*, 1996, **35**, 5404–5417.

17 Z. Otwinowski and W. Minor, *Methods Enzymol.*, 1997, **276**, 307–326.

18 P. Emsley and K. Cowtan, *Acta Crystallogr., Sect. D: Biol. Crystallogr.*, 2004, **60**, 2126–2132.

19 G. N. Murshudov, A. A. Vagin and E. J. Dodson, *Acta Crystallogr., Sect. D: Biol. Crystallogr.*, 1997, **53**, 240–255.

20 R. A. Laskowski, M. W. MacArthur, D. S. Moss and J. M. Thornton, *J. Appl. Crystallogr.*, 1993, **26**, 283–291.

21 E. Krissinel and K. Henrick, *Acta Crystallogr., Sect. D: Biol. Crystallogr.*, 2004, **60**, 2256–2268.

22 W. L. Delano*The Pymol Molecular Graphics System*2002, www.pymol.org.

